Supporting Information

Exfoliation of 2D materials: The role of entropy

*Wei Cao[1,2], Jin Wang[3,4], Ming Ma[*1,2,3]*

[1] State Key Laboratory of Tribology, Tsinghua University, Beijing, 100084, China

[2] Department of Mechanical Engineering, Tsinghua University, Beijing 100084, China

[3] Center for Nano and Micro Mechanics, Tsinghua University, Beijing 100084, China

[4] Department of Engineering Mechanics, Tsinghua University, Beijing 100084, China

*E-mail: maming16@mail.tsinghua.edu.cn

In this supplementary information, we provide additional details on certain aspects of the study reported in the manuscript. The following issues are discussed:

1. Details of simulation models and methods

A. Force field parameters in MD simulations

B. The interlayer potential energy and binding energy

C. The steered molecular dynamics (SMD) methods

D. The thermodynamics integration (TI) methods

E. The averaged force of a sheet suffered by water and the other sheet in the reaggregation process

F. The validity of the choice of the reaction coordinate in exfoliation and reaggregation

2. The density profile of water confined between two nanosheets

3. The angle profile of water confined between two nanosheets

4. The temperature effect on free energy barrier

5. The hydrogen bonds of confined water

6. Diffusion coefficient of confined water

1. Details of simulation models and methods.

A. Force field parameters in MD simulations.

Water was modeled by using the non-polarizable rigid SPC/E model.[1] Bond lengths and angles in water molecules were constrained using the SHAKE algorithm.[2] The inter-atomic interactions for graphene and hBN were described using the Tersoff potential[3-4], and for MoS_2 the Reactive Empirical Bond Order potential[5] was used. The interactions between graphene layers was described from Cheng and Steel.[6] Force field reported by Shih *et al.*[7] was applied to simulate the water-graphene interaction. Carbon atoms in graphene were treated as uncharged interaction sites. The interaction between hBN layers was taken from Won *et al.*, which was modeled by considering the partial charges on B and N.[8] Layered MoS_2 with 2H phase interacts with water according the parameters reported by Heiranian *et al.*[9] The coulombic interaction was not calculated, due to the negligible role of electrostatic interactions for water-MoS_2 system.[10] The cross-term interactions were estimated using the Lorentz−Berthelot mixing rules. The Lennard-Jones potential and electrostatic interactions were both truncated at a distance of 1.2 nm. Long-range electrostatic interactions were calculated with the particle−particle particle−mesh (PPPM) method.[11]

The force field parameters applied in this work were list in table S1. C, B, N, Mo, S, O, and H represent the carbon, boron, nitrogen, molybdenum, sulfur, oxygen, and hydrogen atoms from graphene, hexagonal boron nitride (hBN), molybdenum disulfide (MoS_2), and water, respectively.

Table S1. LJ parameters used in MD simulations for all atomic pairs.

Atom pair	C-C	C-O	O-O	X^a-H
ε (meV)	2.417	4.038	6.744	0.0
σ (Å)	3.4	3.283	3.166	0.0
B-B	N-N	B-N	B-O	N-O
4.117	6.283	5.086	5.270	6.510
3.453	3.365	3.409	3.310	3.267

Mo-Mo	S-S	Mo-S	Mo-O	S-O
0.586	20.016	3.425	1.988	11.619
4.200	3.130	3.665	3.683	3.418

a: X represents interaction sites except H.

B. The interlayer potential energy and binding energy.

We first calculated the binding energy between AB stacked graphene monolayers, which is $E_b = 1.54$ eV/nm^2, and lies within the range reported in both theoretical and experimental works[12]. The binding energy of infinite hBN AA' stacked double layer is $E_b = 3.01$ eV/nm^2. This value is larger than those reported in Ananth et al.[13], and is comparable to that calculated by density functional theory with PBE-D function[14]. We also found $E_b = 1.7$ eV/nm^2 for 2H phase MoS$_2$ double layer. The value is validated by comparing with the other reported data.[15-16]

The potential energy surfaces of water on three kinds of single-layer materials were reported in Figure S1. One water molecule is used as a probe to scan the potential energy of water-layer, in the plane parallel to the sheet. The potential energy for a water adsorbed on graphene, MoS$_2$, and hBN is -62.3, -62.2, and -87.8 meV. The energy barrier along the plane of sheets is calculated to be 2.9, 9.2, and 18.1 meV.
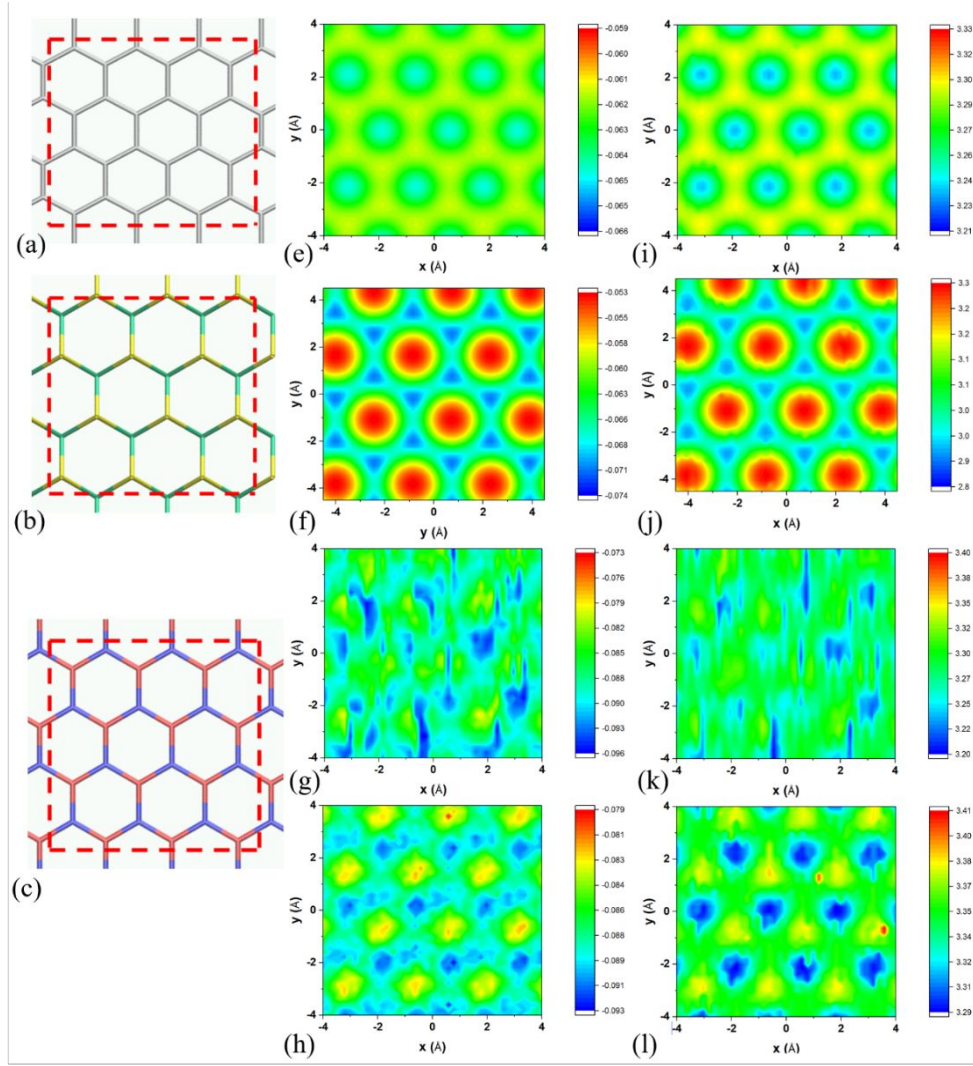
Figure S1. The potential energy surfaces of water on three kinds of nanosheets: graphene (e), MoS_2 (f), and hBN (g, h). The unit of the color bar is eV. The center of mass displacements of the water molecule: graphene (i), MoS_2 (j), and hBN (k, l). The unit of the color bar is Å. For hBN, h and l are the results when the rotation of water is constrained. The ranges along x and y in the figures corresponds to the scopes in the red dashed lines, shown in (a), (b), and (c), represents graphene, MoS_2, and hBN, respectively. Atoms of carbon, boron, nitrogen, molybdenum, and sulfur are shown in silver, red, blue, green, and yellow, respectively.

C. The steered molecular dynamics (SMD) methods.

The potential of mean force (PMF) curves in this work have been calculated using the LAMMPS packages[17]. For the peeling exfoliation, pulling the upper layer of each

kind of 2D materials along the direction perpendicular to the lower layer have been addressed. The schematic is shown in Figure S2. Initially wo monolayers with a side length of 2 nm in the x-y plane were placed in the center of a water box with the dimension of $6 \times 6 \times 8$ nm. Periodic boundary conditions were applied in all three dimensions. The materials were treated as rigid bodies when omitting the entropy effect of sheets. While the investigation of flexibility effect, the rims of both layers were kept frozen, with the other parts being free to vibrate. We performed two exfoliation process, *i.e.* peeling and shearing (Figure S2).

In the SMD simulations, a harmonic constraint (with a spring constant $k = 1$ eV/Å^2) was attached to the center of mass of one edge of a nanosheet with a constant velocity, i.e. $v = 1$ m/s. The PMF is calculated to be the reversible work required to pull one layer from the other layer. Because there are no transition states in the two process, this method is suitable for the calculations. Each simulated system was first equilibrated at 300 K and 1.0 bar for 1 ns in the NPT ensemble with Nose-Hoover barostat and thermostat. The dynamics of Newton's equation were iterated using a 1.0-fs time step. The system was allowed to further relax for 1 ns in the NVT ensemble. Finally, a 3-ns production run was used for data analysis including the PMF calculations. The method is validated by performing simulations with different pulling velocity and spring constant. The reversibility of the exfoliation process is also studied by performing the retraction process, *i.e.* from two separated nanosheets to a binding state.

Peeling exfoliation

Shearing exfoliation
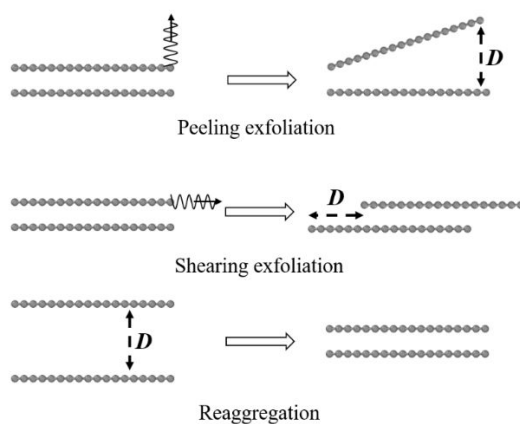
Reaggregation

Figure S2. Schematic of peeling, shearing exfoliation, and reaggregation process. *D* is shown as the reaction coordinate.

(1). The velocity and spring constant effect

We performed SMD methods to model the exfoliation of two graphene nanosheets for different pulling velocity. The PMF curves shown in Figure S3a show the similar free energy tendency. A large velocity would drive the exfoliation process to a non-equilibrium state, leading to a Jarzynski's inequality, where the free energy does not equal to the reversible work in isothermal simulations. The velocity studied in this work, i.e. 1 m/s, is sufficient to reveal the free energy barrier. We also find a small spring constant would cause a large thermal fluctuation, and a large spring constant would tend to destabilize the system (see Figure S3b). Thus, we chose the spring constant described in the methods.
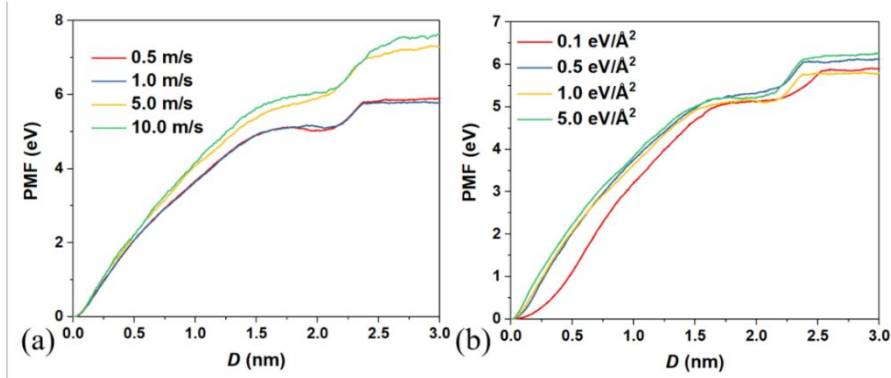

Figure S3. The PMF of water-assisted peeling exfoliation with flexible model graphene double-layers at (a) different pulling velocity and (b) different spring constant.

(2). Comparison of pullout and retraction process.

We explored the reverse process of the peeling and shearing exfoliation of graphene double-layers, i.e. pulling the separated nanosheets back to the binding state. The PMF as a function of pulling distance is shown in Figure S4. The largely overlap of these curves shows a quasi-equilibrium of the steered simulations, indicating the validity of the free energy calculated by this method. For shearing two flexible nanosheets, the retraction deviates from the pullout one a little. This might due to the large shear stress (~0.1 GPa) resulted from the commensurability-dependent stick-slip friction[18]. The deviation in the shearing process further causes the poor linearity of free energy dependent on temperature. We also noted that the site-to-site interaction between

nanosheets is not sufficient to describe the heterogeneous interaction during the shear process[19]. Thus in this work, we do not report the entropy penalty in the shearing exfoliation.
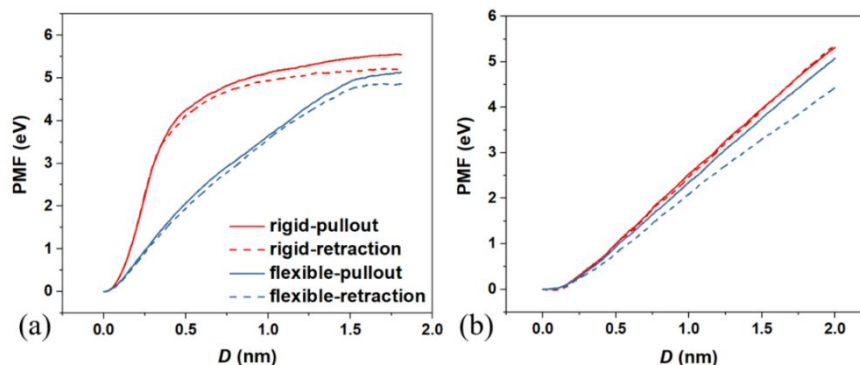

Figure S4. The pullout and retraction of the (a) peeling and (b) shearing exfoliation of graphene double layers.

D. The thermodynamics integration (TI) methods.

To study the PMF in the reaggregation process of exfoliated 2D nanosheets, we performed simulation by numerically integrating the forces of the two monolayers at various intersheet separations (see Figure S2). The PMF was then obtained by integrating the averaged force of nanosheets along a certain range of reaction coordinate. We also attempted to calculate PMF by umbrella-sampling methods. However, the mutual orientation of 2D materials sheets is never parallel after the exfoliation has been initiated, especially when D was less than 0.6 nm. It's difficult to either define the reaction coordinate or set the force constant.

We also compare our results with the method proposed in Adam *et al.*[20], namely, the corresponding distances method (CDM). The binding energy between two graphene layers, predicted from the red curve of Figure S5, is 1.5 eV/nm^2 (the first energy minimum), which equals to that reported in part B. The energy calculated in this work is smaller than that, mainly due to the slightly large gap between two reaction coordinates, and the finite size model. Although the weakness of the parallel sheet method exists, this method provides the opportunity to study the flexibility effect on the reaggregation of 2D materials.
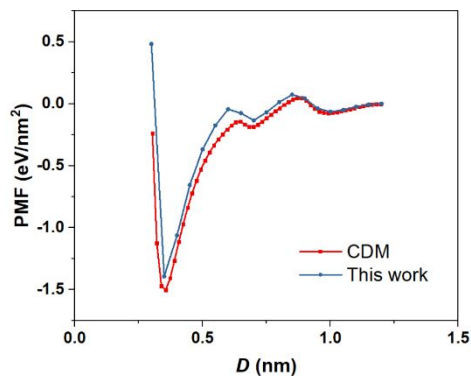
Figure S5. PMF of the reaggregation of two graphene nanosheets (rigid models) in water, computed by the CDM and in this work.

E. The averaged force of a sheet suffered by water and the other sheet in the reaggregation process.

The force on layers are calculated to obtain the PMF results. We both provide the total force and water-induce force in every reaction coordinate. It is obvious to find two energy maxima when the double-layered 2D materials immersed in water. The two windows correspond to the states that single- or two- water layers just fulfill the slits.
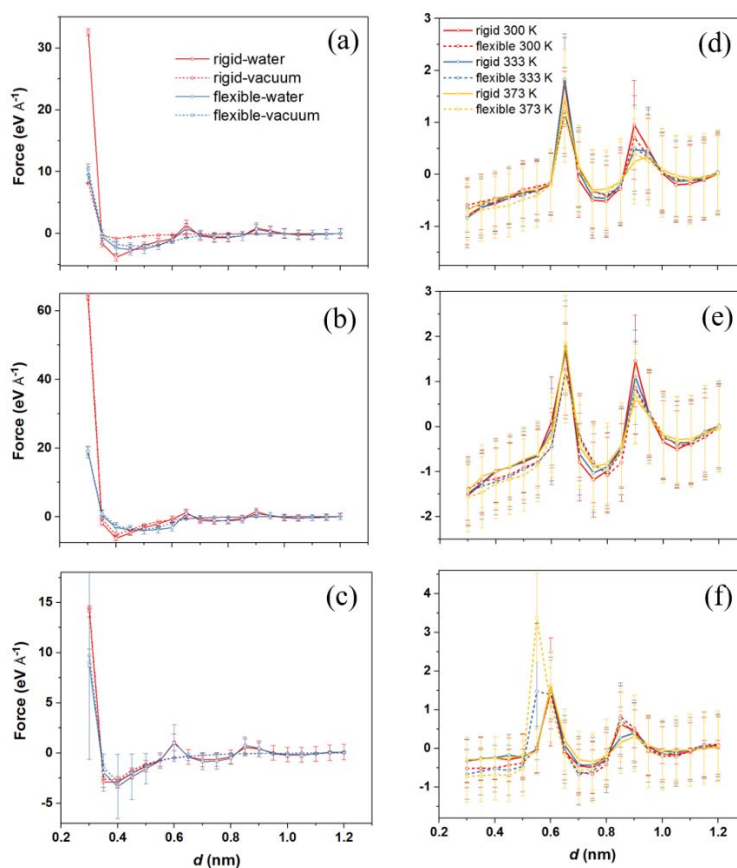
Figure S6. The averaged force of graphene (a, d), hBN (b, e), and MoS_2 (c, f) in water and in vacuum. Panel a, b, and c are the total force includes the contribution of layer-layer and water-layer force at 300 K; panel d, e, and f are the force induced by water at different temperature.

F. The validity of the choice of the reaction coordinate in exfoliation and reaggregation.

The processes in LPE studied in this work has been separated to exfoliation and reaggregation. The initial binding state and final separated state of the exfoliation correspond to the final and initial state of the reaggregation states, respectively. We suppose that the exfoliation and reaggregation would follow different pathways, as described in the text. The simulation protocol would probably be misleading, *e.g.* how can two states present two different values of the free energy from the equilibrium distribution? To elucidate the question, we compare the PMF profiles by taking graphene as an example. In Figure S7, the slope of the curves (force) at initial separations of reaggregation is larger than that of exfoliation, leading to the more favorable route exfoliation through peeling than pulling through the reverse route of reaggregation. After exfoliation, the nanosheets would find a minimum energy path to aggregate in water. The shadow area in Figure S7 shows the PMF at the similar distances between nanosheets among the two processes. We find energy minima in Figure S7a rather than S7b. Hence, besides the orthogonal nanosheets, two tilted nanosheets probably form an energy minimum state, *i.e.* the sheet-water-sheet sandwich structure. The sandwich structure has also been reported in simulation[21] and experiments[22].
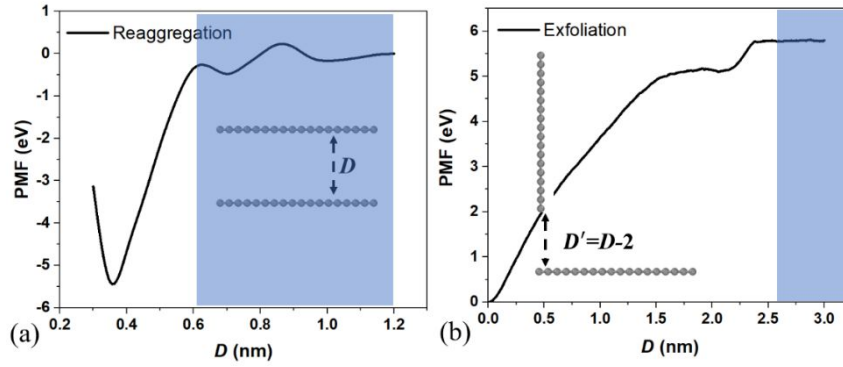
Figure S7. The PMF as a function of D in the exfoliation (b) and reaggregation (a) process for graphene in water at 300 K. The shadow areas represent the PMFs at D ranges from 0.6 to 1.2 nm. For exfoliation, the area shows the distance between the edge of the upper nanosheets and the lower nanosheet. The side length of the nanosheet is ~2 nm.

To further support the statement, we calculated the PMF of nanosheets in water for the aggregation of two tilted nanosheets, as seen in Figure S8a. The free energy barrier for the desorption of water decreases with the increasing angle. For example, the energy barrier decreases to $\sim 3k_BT$ per nm^2 for $\theta = 20°$. We then explored the normal force (pressure) exerted on the graphene nanoplates by water as a function of angle between two nanoplates. Note that a positive means the existence of energy minimum state (or metastable state). In Figure S8b, the normal pressure declines sharply and is estimated to reduce to zero at $\theta \approx 33°$ by linear fitting. It is expected that the metastable state would not be found for $\theta > 33°$. For $\theta < 33°$, the tilted nanosheets would tend to be parallel to each other due to the unbalanced force at different interlayer distance, when the upper nanosheet faces the repulsive force from water. Thus, the reaction coordinates we supposed to be the reaggregation process is reasonable.
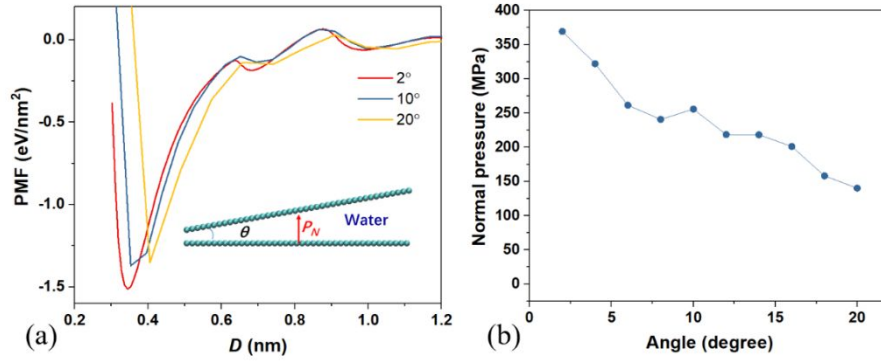
Figure S8. (a) The PMF of two tilted graphene nanosheets in water. The reaction coordinated D is the center of mass distance between two nanosheets. (b) The normal pressure as a function of angle between two graphene nanosheets.

## 2. The density profile of water confined between two nanosheets.

We calculate the density of water in different reaction coordinates. The difference between results for rigid and flexible models mainly at a separation where the force reaches the maximum (Figure S6). For example, the density profile becomes more discontinuous for water in flexible sheets, especially at the lowest density of layered water, *i.e.* 0.8-0.85 nm, which is regarded as a transition state.
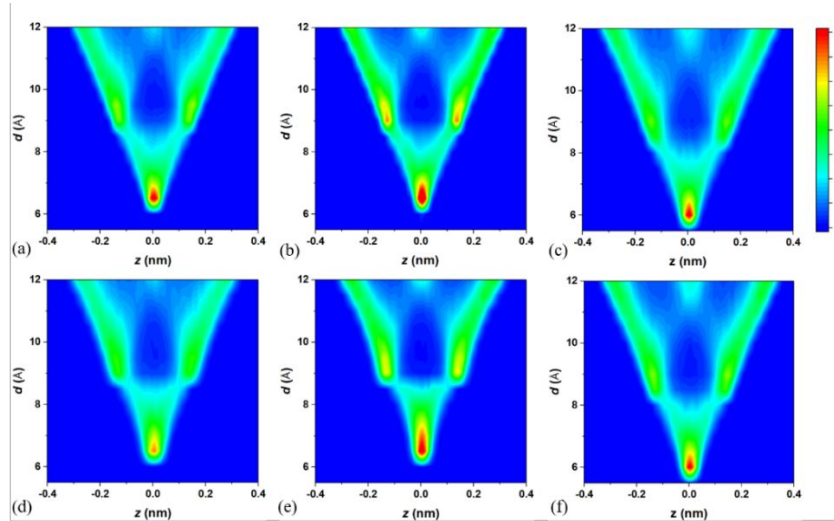
Figure S9. Density profile of water along the direction normal to the layer (graphene: a and d; hBN: b, e; MoS$_2$: c, f). Panel a, b, and c denote the rigid layers; while d, e, and f denote the flexible models. The value of color denotes the density of water with respect to the bulk water density.

3. The angle profile of water confined between two nanosheets.

The angle profile of water along the directions normal to and parallel to the nanosheets are analyzed. With the distribution of orientation, we find the inconsistence for water in the transition state at d = 0.8-0.85 nm. It is worth noting that the dipole orientation hardly changes when considering the lattice vibration of materials.
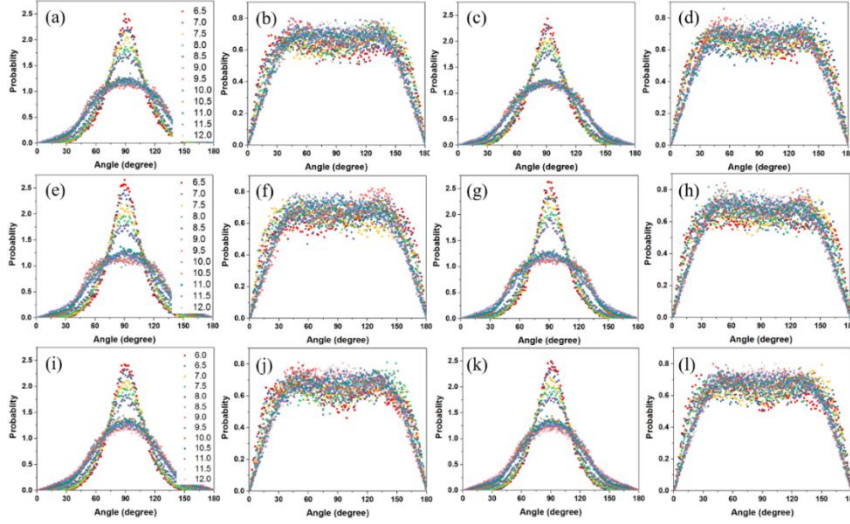

Figure S10. The orientation of water inside two layers at 300 K. The averaged orientation of water confined in double-layered nanosheets. The 1st, 2nd, and 3rd line is for graphene, hBN, and MoS$_2$, respectively. The 1st, 2nd, 3rd and 4th column is for water orientation along the xy plane (parallel to the nanosheets) in rigid models, along z direction (normal to the nanosheets) in rigid models, along the xy plane in flexible models, and along the z direction in flexible models.

4. The temperature effect on free energy barrier.

The entropy is calculated as $\Delta S = -d(\Delta G)/dT$. The free energy difference ΔG at a given temperature T is calculated as the difference between the maximum and minimum of PMF during the exfoliation or aggregation process. Then by calculating ΔG at different temperature T and performing linear fitting for ΔG vs T, one could get ΔS as the negative slope and ΔH as the intercept.

The free energy barrier, ΔG, in the reaggregation process as a function of temperature is shown Figure S11. The data are taken from the energy barrier for the desorption of double-layer water. The linear relationship is observed. We then

calculated the ΔS, which is the negative slope of the fitting line. It is obvious that the slope of rigid model is less than that of flexible one for graphene and hBN. For MoS_2, the result is opposite to those two cases. In addition, we found the difference between flexible and rigid models diminishes at high temperatures for graphene and hBN, and at low temperatures for MoS_2. We also found ΔG for flexible hBN is less than that for MoS_2 at a temperature larger than ~355K. These results arise from the entropy penalty.
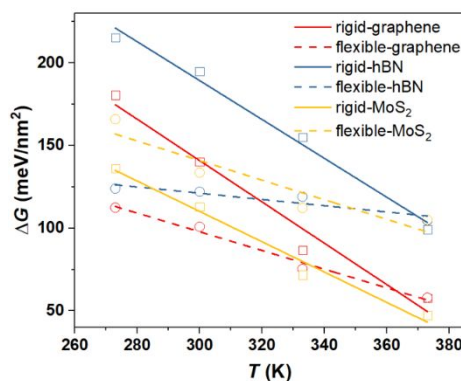
Figure S11. The free energy barrier, ΔG, in the reaggregation process as a function of temperature. The lines show the linear fitting of the data.

### 5. The hydrogen bonds of confined water.

Hydrogen bond (hbond) networks are often used to analyze the confined water properties. As shown in Figure S12, we calculated both the number of hbond per water molecule ($<n_{HB}>$) and hbond relaxation time ($<\tau_{HB}>$) for water confined in two monolayer nanosheets. Along with the intercalation of water diffusing or flowing into the slits, $<n_{HB}>$ would decrease compared to bulk water. During the aggregation process, $<n_{HB}>$ shows a non-monotonic dependence on interlayer distance d. The quantity $<\tau_{HB}>$ is analyzed to characterize the stability of hbonds. For water molecules under tight confinement, *e.g.* water in carbon nanotubes[23] and graphene sheets[24] with $d = 0.65$ nm, they would diffuse as clusters. In these situations, the hbond network is very stable. The stable hbond networks would further restrict the self-diffusion of confined water.
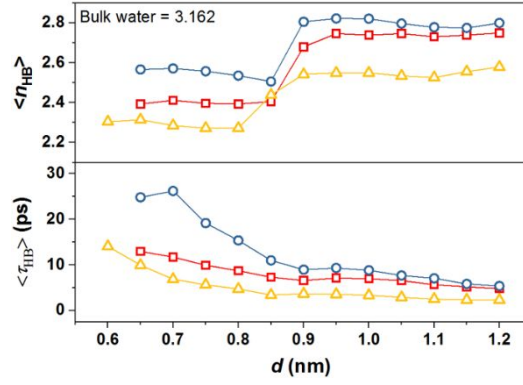
Figure S12. Averaged number ($<n_{HB}>$) and relaxation time (τ_{HB}) of hydrogen bond (hbond) of water as a function of interlayer distance.

6. Diffusion coefficient of confined water.

Figure S13 shows the water diffusion at 300 K. It is obvious to find that the enhancement of water diffusion in graphene layers as a result of lattice vibration. Instead, the diffusion in flexible MoS_2 sheets is less than that in rigid models. On the one hand, the roughness induced by a flexible model would hinder the movement of confined water[25]. On the other hand, water diffusion could be enhanced when the movement of water couples with the vibration of solid surfaces[26]. This coupling effect is suitable for the graphene-water system. While for MoS_2, the roughness effect is dominated. For hBN, For hBN, the influence of flexibility on water diffusion is less than the other two materials.
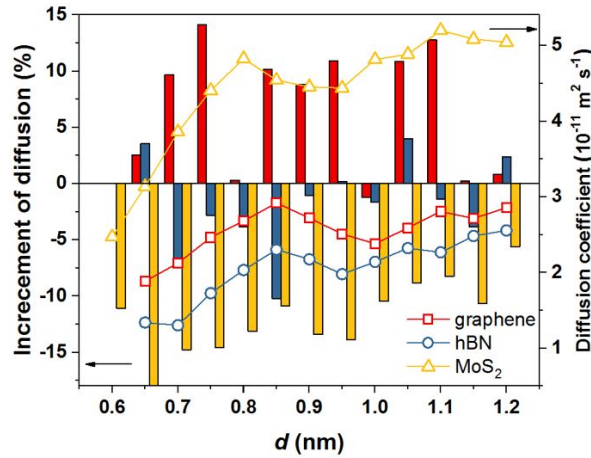
Figure S13. The diffusion coefficient of confined water and increment of values for flexible models upon rigid ones, given by $D_{flexible}/D_{rigid}$ -1.

References.

1. Berendsen, H. J. C.; Grigera, J. R.; Straatsma, T. P. The Missing Term in Effective Pair Potentials. *J. Phys. Chem.* **1987,** *91* (24), 6269-6271.

2. Ryckaert, J. P.; Ciccotti, G.; Berendsen, H. J. Numerical Integration of the Cartesian Equations of Motion of A System with Constraints: Molecular Dynamics of n-Alkanes. *J. Comput. Phys.* **1977,** *23* (3), 327-341.

3. Lindsay, L.; Broido, D. Optimized Tersoff and Brenner Empirical Potential Parameters for Lattice Dynamics and Phonon Thermal Transport in Carbon Nanotubes and Graphene. *Phys. Rev. B* **2010,** *81* (20), 205441.

4. Sevik, C.; Kinaci, A.; Haskins, J. B.; Çağın, T. Characterization of Thermal Transport in Low-Dimensional Boron Nitride Nanostructures. *Phys. Rev. B* **2011,** *84* (8), 085409.

5. Liang, T.; Phillpot, S. R.; Sinnott, S. B. Parametrization of a Reactive Many-Body Potential for Mo–S Systems. *Phys. Rev. B* **2009,** *79* (24), 245110.

6. Cheng, A.; Steele, W. A. Computer Simulation of Ammonia on Graphite. I. Low Temperature Structure of Monolayer and Bilayer Films. *J. Chem. Phys.* **1990,** *92* (6), 3858-3866.

7. Shih, C. J.; Lin, S.; Strano, M. S.; Blankschtein, D. Understanding the Stabilization of Liquid-Phase-Exfoliated Graphene in Polar Solvents: Molecular Dynamics Simulations and Kinetic Theory of Colloid Aggregation. *J. Am. Chem. Soc.* **2010,** *132* (41), 14638-14648.

8. Won, C. Y.; Aluru, N. R. Water Permeation Through A Subnanometer Boron Nitride Nanotube. *J. Am. Chem. Soc.* **2007,** *129* (10), 2748-2749.

9. Heiranian, M.; Farimani, A. B.; Aluru, N. R. Water Desalination with A SingleLayer MoS_2 Nanopore. *Nat. Commun.* **2015,** *6*, 8616

10. Rajan, A. G.; Sresht, V.; Padua, A. A. H.; Strano, M. S.; Blankschtein, D. Dominance of Dispersion Interactions and Entropy over Electrostatics in Determining the Wettability and Friction of Two-Dimensional MoS_2 Surfaces. *Acs Nano* **2016,** *10* (10), 9145-9155.

11. Darden, T.; York, D.; Pedersen, L. Particle Mesh Ewald: An N· log (N) Method for Ewald Sums in Large Systems. *J. Chem. Phys.* **1993,** *98* (12), 10089-10092.

12. Sinclair, R. C.; Suter, J. L.; Coveney, P. V. Graphene-Graphene Interactions: Friction, Superlubricity, and Exfoliation. *Adv. Mater.* **2018,** *30* (13), e1705791.

13. Govind Rajan, A.; Strano, M. S.; Blankschtein, D. Ab Initio Molecular Dynamics and Lattice Dynamics-Based Force Field for Modeling Hexagonal Boron Nitride in Mechanical and Interfacial Applications. *J. Phys. Chem. Lett.* **2018**, 1584-1591.

14. Bjorkman, T.; Gulans, A.; Krasheninnikov, A. V.; Nieminen, R. M. van der Waals Bonding in Layered Compounds from Advanced Density-Functional First-Principles Calculations. *Phys. Rev. Lett.* **2012,** *108* (23), 235502.

15. Sresht, V.; Rajan, A. G.; Bordes, E.; Strano, M. S.; Padua, A. A. H.; Blankschtein, D. Quantitative Modeling of MoS_2-Solvent Interfaces: Predicting Contact Angles and Exfoliation Performance using Molecular Dynamics. *J. Phys. Chem. C* **2017,** *121* (16), 9022-9031.

16. Fuhr, J.; Sofo, J.; Saúl, A. Adsorption of Pd on MoS_2 (1000): Ab initio Electronic-

Structure Calculations. *Phys. Rev. B* **1999,** *60* (11), 8343.

17. Plimpton, S. Fast Parallel Algorithms for Short-Range Molecular Dynamics. *J. Comput. Phys.* **1995,** *117* (1), 1-19.

18. Chen, X.; Yi, C.; Ke, C. Bending Stiffness and Interlayer Shear Modulus of Few-Layer Graphene. *Appl. Phys. Lett.* **2015,** *106* (10), 101907.

19. Leven, I.; Maaravi, T.; Azuri, I.; Kronik, L.; Hod, O. Interlayer Potential for Graphene/h-BN Heterostructures. *J. Chem. Theory Comput.* **2016,** *12* (6), 2896-2905.

20. Hardy, A.; Dix, J.; Williams, C. D.; Siperstein, F. R.; Carbone, P.; Bock, H. Design Rules for Graphene and Carbon Nanotube Solvents and Dispersants. *ACS Nano* **2018**, *12* (2), 1043-1049.

21. Lv, W.; Wu, R. The Interfacial-organized Monolayer Water Film (MWF) Induced "Two-Step" Aggregation of Nanographene: Both in Stacking and Sliding Assembly Pathways. *Nanoscale* **2013**, *5* (7), 2765-2775.

22. Verguts, K.; Schouteden, K.; Wu, C. H.; Peters, L.; Vrancken, N.; Wu, X.; Li, Z.; Erkens, M.; Porret, C.; Huyghebaert, C. *et al*. Controlling Water Intercalation Is Key to a Direct Graphene Transfer. *ACS Appl. Mater. Interfaces* **2017**, *9* (42), 37484-37492.

23. Cao, W.; Huang, L.; Ma, M.; Lu, L.; Lu, X. Water in Narrow Carbon Nanotubes: Roughness Promoted Diffusion Transition. *J. Phys. Chem. C* **2018,** *122* (33), 19124-19132.

24. Jiao, S.; Xu, Z. Non-Continuum Intercalated Water Diffusion Explains Fast Permeation through Graphene Oxide Membranes. *ACS Nano* **2017,** *11* (11), 11152-11161.

25. Daub, C. D.; Wang, J.; Kudesia, S.; Bratko, D.; Luzar, A. The Influence of Molecular-scale Roughness on the Surface Spreading of an Aqueous Nanodrop *Faraday Discuss.* **2010,** *146*, 67-77.

26. Ma, M.; Tocci, G.; Michaelides, A.; Aeppli, G. Fast Diffusion of Water Nanodroplets on Graphene. *Nat. Mater.* **2016,** *15* (1), 66-71.